ChemPubSoc Europe

DOI: 10.1002/open.201600064

Open Access ChemistryOPEN Full Papers

Mechanistic Investigation into Olefin Epoxidation with H_2O_2 Catalyzed by Aqua-Coordinated Sandwich-Type Polyoxometalates: Role of the Noble Metal and Active Oxygen Position

Chenggang Ci,[a, b, c] Hongsheng Liu,[b] Likai Yan,*[a] and Zhongmin Su*[a]

Aqua-coordinated sandwich-type polyoxometalates (POMs), $\{[WZnTM_2(H_2O)_2](ZnW_9O_{34})_2\}^{n-}$ (TM=Rh^{III}, Pd^{II}, and Pt^{II}), catalyze olefin epoxidation with hydrogen peroxide and have been well established, and they present an advance toward the utilization of olefins. To elucidate the epoxidation mechanism, we systematically performed density functional calculations. The reaction proceeds through a two-step mechanism: activation of H_2O_2 and oxygen transfer. The aqua-coordinated complexes show two distinct H_2O_2 activation pathways: "two-step" and "concerted". The concerted processes are more facile and proceed with similar and rate-determining energy barriers at the Rh-, Pd-, and Pt-containing transition states, which agrees well with the experimental results. Next, the resulting TM–OH–(μ-OOH) intermediate transfers an O atom to olefin to form an epoxide. The higher reactivity of the Rh-containing POM is attributed to more interactions between the Rh and hydroperoxo unit. We also calculated all active oxygen positions to locate the most favorable pathway. The higher reactivity of the two-metal-bonded oxygen position is predominantly ascribed to its lower stereoscopic hindrance. Furthermore, the presence of one and two explicit water solvent molecules significantly reduces the energy barriers, making these sandwich POMs very efficient for the olefin epoxidation with H_2O_2.

1. Introduction

The olefin epoxidation with hydrogen peroxide has been extensively studied for several decades and still is a challenge for complicated polymetallic complexes.[1–5] As epoxides are a useful raw material, they have a common application in the synthesis of functionalized organic compounds, such as surfactants, medicine, paints, and so forth.[1–5] Hydrogen peroxide, as an active oxygen-rich donor, has a relatively cheap price and forms water as it's only by product.[6–9] However, the energy of the O–O bond has reached approximately 50 kcal mol^{-1}, thus the search for an environmentally friendly catalyst has received significant attention.[10,11]

Polyoxometalates (POMs), as abundant molecular-based inorganic materials, are potentially interesting catalysts for the epoxidation of olefins.[12–40] Particular attention has been paid to transition-metal-substituted polyoxotungstates, which have shown significant catalytic activity and selectivity, such as Venturello-type anions, $\{PO_4[WO(O_2)_2]_4\}^{3-}$,[15–17] Keggin-type[18–29] and Tourné sandwich-type polyoxotungstates.[30–40] In the literature, the low-valent noble transition-metal-substituted sandwich-type polyoxotungstates, $\{[WZnTM_2(H_2O)_2](ZnW_9O_{34})_2\}^{n-}$ (TM=Rh^{III}, Pd^{II}, and Pt^{II}), referred to as **1 Rh**, **1 Pd**, and **1 Pt** (Figure 1), have been reported to be highly active and selective catalysts with a good solvolytic stability for olefin epoxidation with H_2O_2.[39]

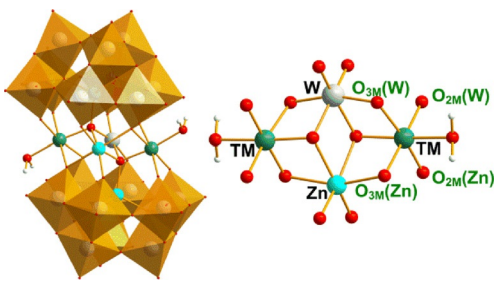

Figure 1. Polyhedral/ball-and-stick representation of $[(WZnTM_2(H_2O)_2)(ZnW_9O_{34})_2]^{n-}$ (TM=Rh^{III}, Pd^{II}, and Pt^{II}).

[a] Dr. C. G. Ci, Prof. Dr. L. K. Yan, Prof. Dr. Z. M. Su
Institute of Polyoxometalate Chemistry
Department of Chemistry, Northeast Normal University
Changchun, Jilin 130024 (P. R. China)
E-mail: yanlk924@nenu.edu.cn
zmsu@nenu.edu.cn

[b] Dr. C. G. Ci, Prof. Dr. H. S. Liu
School of Chemistry and Chemical Engineering
Daqing Normal University, Key Laboratory of Oilfield Applied Chemistry
College of Heilongjiang Province, Daqing 163712 (P. R. China)

[c] Dr. C. G. Ci
Department of Chemistry and Chemical Engineering
Qiannan Normal University for Nationalities
Duyun 558000 (P. R. China)

Supporting Information for this article can be found under http://dx.doi.org/10.1002/open.201600064.

According to previous reports on the epoxidation by POMs, the catalytic reaction proceeded through a two-step mechanism: 1) activation of H_2O_2 and 2) oxygen transfer; in addition, three distinct H_2O_2 activation mechanism have been reported.[24–29] Musaev and co-workers reported a divanadium-substituted POM, $[\gamma\text{-}1,2\text{-}H_2SiV_2W_{10}O_{40}]^{4-}$, which contained a core of $[OV\text{–}(\eta\text{-}OH)_2\text{–}VO]$.[24] They proposed a peroxo-type mechanism, that is, the heterolytic cleavage of H_2O_2 forms a $[OV\text{–}(\eta\text{-}OOH)(\text{–}OH)\text{–}VO]$ peroxo intermediate, and then the oxygen transfer is performed favorably through a 'water-assisted' pathway (Scheme 1).

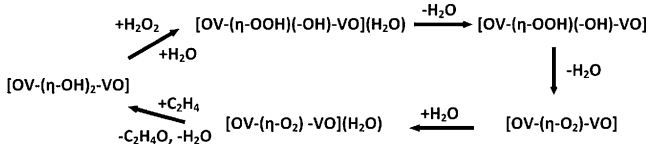

Scheme 1. Epoxidation mechanism based on the divanadium-substituted polyoxometalate, $[\gamma\text{-}1,2\text{-}H_2SiV_2W_{10}O_{40}]^{4-}$.[24]

For the second type, several computational studies have reported the lacunary-substituted POM, $[\gamma\text{-}H_2SiW_{10}O_{36}]^{4-}$,[25] as well as mono- and dititanium-substituted POMs $[PTi(OH)W_{11}O_{39}]^{4-}$ and $[Ti_2(OH)_2As_2W_{19}O_{67}(H_2O)]^{8-}$.[26–29] A two-step mechanism has been proposed. First, the catalytic reaction starts with the heterolytic cleavage of H_2O_2, forming a TM–OOH or TM–OO(μ-OH) intermediate, and then the alpha- or beta-oxygen atom of the intermediates is transferred to the olefin to form an epoxide (Scheme 2).

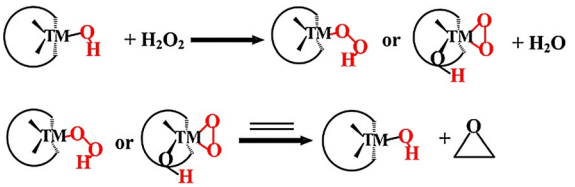

Scheme 2. Epoxidation mechanism based on the mono- and ditransition-metal-substituted polyoxometlates, $[PTM(OH)W_{11}O_{39}]^{4-}$ and $[TM_2(OH)_2As_2W_{19}O_{67}(H_2O)]^{8-}$, TM = Ti, V, Zr, Nb, Mo, W and Re.[26–29]

For the third aqua-coordinated POM type, Neumann et al. have studied Rh-, Pd-, and Pt-substituted sandwich-type POMs $\{[WZnTM_2(H_2O)_2](ZnW_9O_{34})_2\}^{n-}$ ($TM=Rh^{III}$, Pd^{II}, and Pt^{II}).[39] They indicated that the activation of H_2O_2 leads to the formation of a stable TM–OH–(μ-OOH) hydroperoxo-tungstate intermediate, and subsequently determined the reactivity and selectivity. Interestingly, they observed a similar reactivity for each of these three catalysts. Furthermore, they also found that the bridge-oxygen atom of the TM–O–W unit (Figure 2) is the active position, and the three-metal-bonded (TM, W, and Zn) oxygen atom (O_{3M}) is more favorable, owing to the increased electrophilicity. However, because the O_{3M} atom is located inside the TM–O–W triad, the electronic effect will compete with the higher steric hindrance. We know of no reports documenting

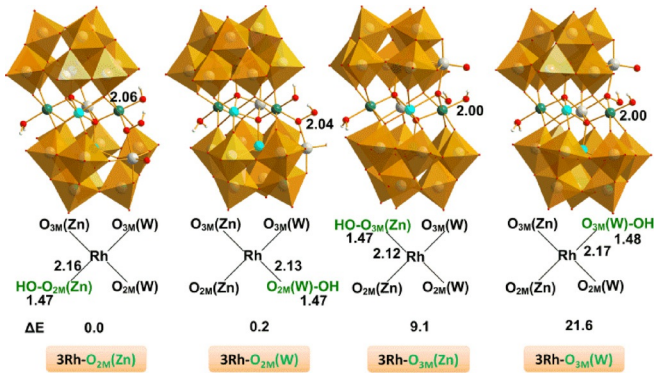

Figure 2. Four isomers of intermediate **3 Rh** with selected bond lengths (in Å). Energy is given in kcal mol^{-1}.

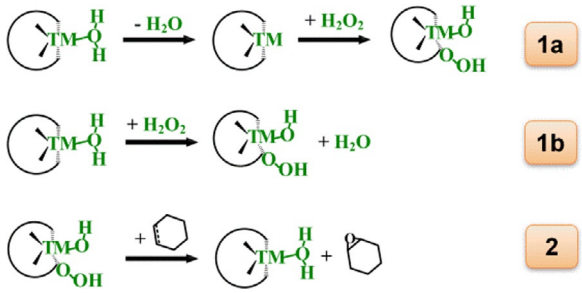

Scheme 3. Proposed epoxidation mechanism based on $\{[WZnTM_2(H_2O)_2](ZnW_9O_{34})_2\}^{n-}$, TM = Rh(III), Pd(II) and Pt(II).

the epoxidation mechanism of olefin with H_2O_2 catalyzed by aqua-coordinated sandwich-type POMs. Thus, we initially hypothesize a mechanism (Scheme 3): step 1, H_2O_2 activation to form the TM–OH–(μ-OOH) intermediate; step 2, oxygen transfer from the intermediate to the olefin to form an epoxide.

The main goal of the present paper is to analyze the viability of the epoxidation mechanism of an olefin catalyzed by aqua-coordinated POMs, $\{[WZnTM_2(H_2O)_2](ZnW_9O_{34})_2\}^{n-}$ ($TM=Rh^{III}$, Pd^{II} and Pt^{II}), including analyses of the roles of the substituted noble metal, active oxygen position, and solvent. Computational analyses of the catalytic mechanism with larger POM systems, such as those reported in this study, remain a challenge for computational chemistry and will be very helpful for evaluating and improving epoxidation catalysts.

2. Results and Discussion

2.1. Structures

The reactants, intermediates, transition states, and products are fully optimized by using the polarizable continuum model (PCM) with water as the solvent; the effect of explicit water molecules will be discussed in the following section. In Rh^{III}-containing local minima, the rhodium center is η^6-coordinated, owing to the d^6 electronic configuration of Rh^{III}, and all of the Rh–O bonds are approximately 2.1 Å in length. However, in most Pd^{II}- and Pt^{II}-containing local minima, owing to the d^8

electronic configuration of Pd^{II} and Pt^{II}, the metal centers are η^5-coordinated and the TM–O_{2M}(Zn) and TM–O_{3M}(W) bond lengths reach more than about 2.7 Å (see the Supporting Information). Herein, we use a Rh-containing POM as the example, and cyclohexene (C_6H_{10}) as the olefin model.

Neumann et al. indicated that the O_{3M} position is more favorable than the O_{2M} position upon H_2O_2 activation, owing to its higher electrophilicity.[39] However, as mentioned above, there is a competition between stereoscopic and electronic effects. To obtain the most facile pathway, we optimized all four intermediates. In Figure 2, around each Rh^{III} center, four kinds of oxygen atom: O_{2M}(W), O_{2M}(Zn), O_{3M}(W), and O_{3M}(Zn) can be attacked by H_2O_2 to form four similar intermediates.

The energy of **3 Rh**–**O_{3M}** is higher than that of **3 Rh**–**O_{2M}** by about 9–22 kcal mol^{-1} (Figure 2), which will lead to a much higher overall energy barrier at the O_{3M} position in the next oxygen-transfer step. Similar results are obtained when the central metal is Pd^{II} or Pt^{II} (Figures S1 and S2). Thus, O_{3M} is not expected to be the active position, that is, the stereoscopic effect will play a more important role. In the following sections, we initially use the O_{2M}(Zn) to discuss the epoxidation mechanism, and the remaining active oxygen positions will subsequently be studied.

2.2. General View of the Energy Profile and Mechanism

As proposed in Scheme 3, this epoxidation reaction can be performed through a two-step mechanism: activation of H_2O_2 (step 1) and oxygen transfer (step 2). For step 1, two possible methods can form the TM–OH–(μ-OOH) intermediate, that is, step 1 a, dissociation of the water ligand and subsequent cleavage of the HO–OH bond, or step 1 b, cleavage of the HO–OH bond accompanied with H abstraction and OH addition. In step 2, the TM–OH–(μ-OOH) intermediate transfers an oxygen atom to the olefin to form an epoxide and to regenerate the catalyst. The calculated potential energy profile is exhibited in Figure 3, showing the electronic energy and free energy. In the following sections, we will describe each step in detail.

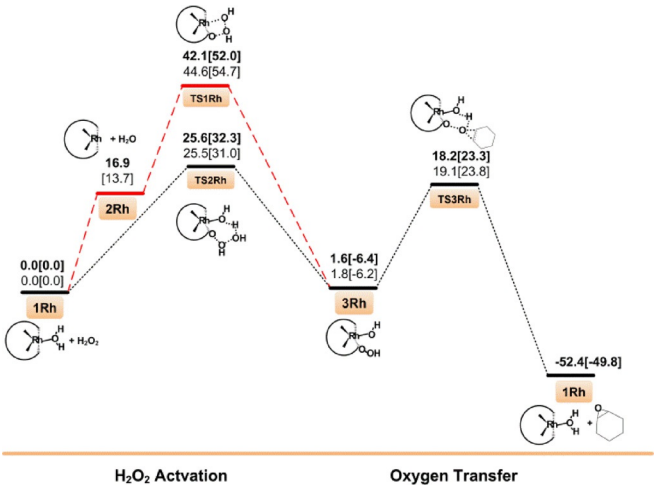

Figure 3. Potential energy profile for olefin epoxidation with Rh-containing POM. Red dashed lines correspond to the less favorable path. Numbers given in bold and plain are calculated relative to the O_{2M}(Zn) and O_{2M}(W) positions, respectively. Electronic energy is given in kcal mol^{-1} (values in parentheses correspond to free energy).

2.3. Activation of H_2O_2

As mentioned above, there are two methods that can activate H_2O_2 (Scheme 3). In step 1 a, starting from reactant **1 Rh**, coordinated H_2O is released to form **2 Rh**. Owing to the similar geometries of **1 Rh**, **1 Pd**, and **1 Pt**, we only softly scanned the dissociation of the water ligand for **1 Rh** (Figure S3). It is shown that this step is an endothermic process, by 16.9 kcal mol^{-1}, and proceeds without an energy barrier. Next, cleavage of the HO–OH bond simultaneously generated two OH moieties bound to Rh^{III} and the O_{2M} atom, respectively, leads to the formation of **3 Rh**. It proceeds with a 25.6 kcal mol^{-1} energy barrier at **TS1Rh** (Figure 4), whereas the overall barrier height reaches 42.1 kcal mol^{-1}. A similar behavior is observed when

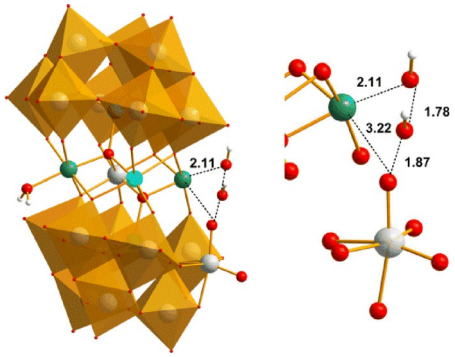

Figure 4. Optimized structure of **TS1Rh** (distances in Å).

the central transition metal is Pd^{II} ($\Delta E = 27.8$ kcal mol^{-1}, overall $\Delta E = 39.5$ kcal mol^{-1}) (Figure S4). Surprisingly, **TS1Pt** has a much lower energy barrier (8.6 kcal mol^{-1}) (Figure S5). The reason can be seen from the reactive center of **TS1Pt**, as one increased intramolecular hydrogen bond is found between the proton of the water ligand and the bridge-oxygen atom of subunit $[ZnW_9O_{34}]^{12-}$ (Figure S6), which reduces the energy barrier of **TS1Pt**. Nevertheless, the overall energy barrier still reaches 31.2 kcal mol^{-1}. In an attempt to reduce the energy barrier of step 1 a, we tried many times to locate similar **TS1Rh** or **TS1Pd** species with more intramolecular hydrogen bonds, but it always leads to the same results. Alternatively, to avoid the artificial effect, we investigated the role of explicit water solvent, which is discussed in the following section. Furthermore, we also tried to find a TM–OO- or TM–OOH-type transition state, for example, the substitution of H_2O by H_2O_2. However, many efforts led to failure, owing to the much higher steric hindrance. Therefore, step 1 a is not a favorable pathway for activating H_2O_2.

Step 1 b is a concerted process (Scheme 3), including the cleavage of a HO–OH bond accompanied by H abstraction and OH addition with two OH moieties, which leads to the formation of **3 Rh** and a H_2O molecule. For simplicity of discus-

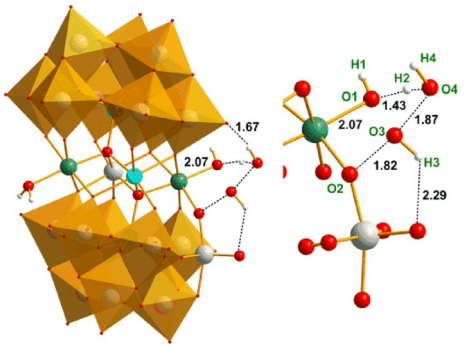

Figure 5. Optimized structure of **TS2Rh** (distances in Å).

sion, denote the process: POM–Rh–$O^1H^1H^2$(μ-O^2) + $H^3O^3O^4H^4$ → POM–Rh–O^1H^1–(μ-$O^2O^3H^3$) + $H^2O^4H^4$.

Step 1 b is calculated to be endothermic by about 2 kcal mol^{-1}. A stable six-membered-ring transition state, **TS2Rh** (Figure 5), is located with an energy barrier of 25.6 kcal mol^{-1}, and the free energy barrier is 32.3 kcal mol^{-1}. All of the calculated important bond parameters (O^3–O^4 = 1.87 Å, O^2–O^3 = 1.82 Å, and H^2–O^4 = 1.07 Å) correspond to the cleavage of the HO–OH bond and the formation of **3 Rh** and a water molecule. The imaginary normal vibration modes of **TS2Rh** also show the corresponding scratching vibration of O^3–O^4, O^2–O^3, and H^2–O^4 bonds.

Furthermore, Pd- and Pt-containing POMs were also studied. Table 1 collects the electronic and free energy barriers as well as some selected bond parameters. It is shown that the energy barriers of these three transition states are about 26 (Δ*E*) or 32 kcal mol^{-1} (Δ*G*) at the O_{2M}(Zn) position. Furthermore, as shown in Figures 3, S4, and S5, the energy barrier of step 1 b is higher than that of step 2 by about 2–14 kcal mol^{-1} (overall Δ*E*) or 2–9 kcal mol^{-1} (overall Δ*G*). Therefore, from an energy point of view, step 1 b is the rate-determining step, which is in good agreement with the experimental observation, that is, the cleavage of H_2O_2 determines the reactivity.[39]

Table 1. Selected bond parameters and energy barriers for **TS2Rh**, **TS2Pd**, and **TS2Pt**.

	TS2Rh		TS2Pd		TS2Pt	
	Zn[a]	W	Zn	W	Zn	W
d(O^2–O^3) [Å]	1.82	1.82	1.84	1.83	1.80	1.86
d(O^3–O^4) [Å]	1.87	1.86	1.86	1.85	1.85	1.85
d(H^2–O^4) [Å]	1.07	1.07	1.06	1.09	1.11	1.07
Δ*E* [kcal mol^{-1}]	25.6	25.5	25.8	30.5	25.5	35.0
Δ*G* [kcal mol^{-1}]	32.3	31.0	32.7	32.1	35.3	40.8

[a] Zn or W corresponds the O_{2M}(Zn) or O_{2M}(W) position, respectively.

2.4. Oxygen Transfer

This step starts with attack of the olefin on intermediate **3 Rh**, and follows the O-atom transfer to form an epoxide and the catalyst, that is, POM–Rh–O^1H^1–(μ-$O^2O^3H^2$) + C_6H_{10} → POM–Rh$O^1H^1H^2$–(μ-O^2) + $C_6H_{10}O^3$. It can be seen that step 2 is typical beta-oxygen transfer from the bridging hydroperoxo moiety to the olefin. Recently, Poblet and co-workers have proposed that the mechanism of Ti–OOH through beta-oxygen has a lower energy barrier for dititanium-substituted sandwich-type POMs.[28,29] As could be expected, this process will proceed with a slightly lower energy barrier; the calculated energy barrier was 16.6 (Δ*E*) or 29.7 kcal mol^{-1} (Δ*G*) at the located transition state, **TS3Rh** (Figure 6).

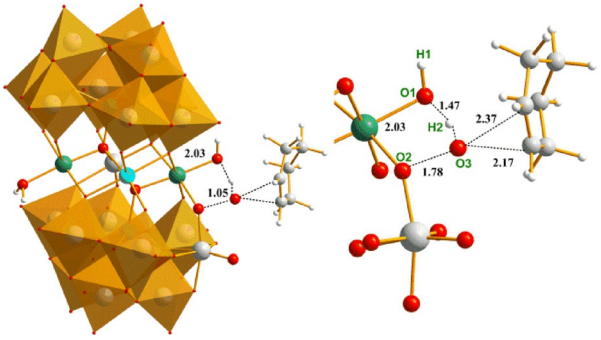

Figure 6. Optimized structure of **TS3Rh** (distances in Å).

In **TS3Rh**, the O^2–O^3 bond length is elongated to 1.78 Å, and the H^2 to O^1 distance decrease from 1.49 to 1.47 Å. It can be seen that the cleavage of the O^2–O^3 bond accompanies the O^3 atom transfers to the olefin, and simultaneously the H^2 proton transfers to the O^1 atom, which leads to the formation of an epoxide and the catalyst. To verify the located transition state, a frequency calculation was performed. The only imaginary normal vibration of **TS3Rh** shows that the O^3 atom oscillates between the O^2 atom and two carbon atoms, and the H^2 atom oscillates between O^3 and O^1 atoms, indicating that **TS3Rh** connects with **3 Rh** and the products, that is, the epoxide and the catalyst. This step was calculated to be exothermic by more than 50 kcal mol^{-1}.

The oxygen-transfer step is performed through nucleophilic attack of the olefin. Thus, the electrons will be transferred from the $\pi_{C=C}$ orbital of the olefin to σ*(O^2–O^3) of the TM–OOH unit. Natural bond orbital (NBO) calculation results (Table 2) show a natural population analysis (NPA) electronic density transfer of about 0.1 e from the olefin to hydroperoxo anions.[45] Previous DFT studies have found that the lower the energy of the σ*(O^2–O^3) orbital, the lower the energy barrier for the alpha-oxygen-transfer process.[41–44] Surprisingly, as for the beta-oxygen-transfer process, we find that the energy barriers of **TS3s** do not follow the latter tend at the O_{2M}–Zn position, that is, **TS3Rh** always has slightly higher energy barriers. To check this, the electric configuration of the central metal was analyzed. In comparison with Pd^{II} {[Kr]$4d^8$} and Pt^{II} {[Xe]$4f^{14}5d^8$}, Rh^{III} {[Kr]$4d^6$} has more empty d orbitals, which helps alpha-O^2 atom transfer the p-electron to the beta-O^3 atom, and it induces O^2–O^3 bond polarization toward the O^2 atom. As a result, in **3 Rh**, the beta-O^3 atom becomes more positively charged in comparison with **3 Pd** and **3 Pt** (Table 2). Thus, the decreased

Table 2. NBO analysis for **3 Rh**, **3 Pd**, and **3 Pt** and oxygen-transfer energy barriers.

	3 Rh		3 Pd		3 Pt	
	Zn[a]	W	Zn	W	Zn	W
$d(O^2–O^3)$ [Å]	1.78	1.78	1.78	1.78	1.78	1.79
$\sigma^*(O^2–O^3)$ [eV]	2.91	3.02	2.81	2.58	2.61	2.48
$q_{NPA}(O^2)$ [au]	−0.358	−0.367	−0.397	−0.400	−0.399	−0.397
$q_{NPA}(O^3)$ [au]	−0.498	−0.497	−0.523	−0.518	−0.522	−0.516
$\Delta q_{NPA}(O^2–O^3)$ [au]	0.14	0.13	0.126	0.118	0.123	0.119
ΔE[b] [kcal mol^{-1}]	16.6	17.3	27.0	21.4	22.7	15.5
ΔG[b] [kcal mol^{-1}]	29.7	30.1	40.5	30.9	36.8	27.5

[a] Zn or W represents the O_{2M}(Zn) or O_{2M}(W) position, respectively. [b] ΔE and ΔG were calculated relative to the **3 TM** intermediate.

charge of distal O^3 will increase the electrophilicity of hydroperoxo group and the activity of **3 Rh**. These reasons also reveal that, in comparison to the cleavage of the O–O bond in the H_2O_2 activation step, the polarization of the O^2–O^3 bond slightly reduces the energy barriers in the epoxidation step. Besides, the lower energy barrier of **TS3Rh** also agrees well with experimental observation of a slightly higher yield of epoxide when the reaction is catalyzed by a Rh-containing POM.[39]

2.5. Role of the Active Oxygen Position

Around each noble-metal center, four active oxygen atoms can be attacked by H_2O_2 (Figure 2). However, many efforts have been made to locate a transition state at the O_{3M} position either for step 1 or step 2, but failed because of the higher stereoscopic hindrance. Besides, as mentioned above, the energy values of intermediates 3 TM–O_{3M} are higher those of 3 TM–O_{2M}. As a result, only O_{2M} positions are available. As step 1 a is unfavorable, we only recalculate step 1 b and step 2. All corresponding geometries were fully optimized at the same level, and details are given in the Supporting Information. In step 1 b, the optimized geometries of transition states at the O_{2M}–W position are similar as those at the O_{2M}–Zn position (Figure S7). The free-energy barrier of **TS2–Rh–O_{2M}W** and **TS2–Pd–O_{2M}W** were slightly reduced by about 1.0 kcal mol^{-1}; however, the barrier of **TS2–Pt–O_{2M}W** increased by about 5 kcal mol^{-1}. Thus, from an the energy point of view, for the Pt-containing POMs, O_{2M}–W is not a facile position for olefin attack.

For step 2, the order of the energy barriers of all transition states at the O_{2M}–W position agrees well with the order of energy for the $\sigma^*(O^2–O^3)$ orbital (Table 2). For example, the order of energies of the $\sigma^*(O^2–O^3)$ orbital (O_{2M}–Zn, 2.91 vs. O_{2M}–W, 3.02 eV) corresponds well with the order of the energy barriers (**TS3Rh–O_{2M}Zn**, 16.6 vs. **TS3Rh–O_{2M}W**, 17.3 kcal mol^{-1}). However, the overall energy barrier of **TS3Pt–O_{2M}W** increases by about 4 kcal mol^{-1} more than that of **TS3Pt–O_{2M}Zn**, owing to the energy discrepancy between **3 Pt–O_{2M}W** and **3 Pt–O_{2M}Zn**. Therefore, the O_{2M}–W position is favored for Rh- and Pd-containing POMs, and the process is not facile for the Pt-containing POM. Nevertheless, from an energy perspective, the step 1 b is still the rate-determining step.

2.6. Water-Assisted Process

As mentioned above, previous theoretical studies proposed that the presence of explicit solvent can significantly reduce the energy barrier caused by intermolecular hydrogen bonds.[24,25] However, as there are 40 water molecules per unit of reactant,[39] it is very expensive to calculate this for all solvents. To identify the position of protonation, an NBO calculation was performed.[45] It is shown that the four bridge-oxygen atoms around the reactive center have a slightly higher negative charge distribution (e.g. O_b, −0.71 au vs. O_t, 0.65 au in **1 Rh**). Therefore, we calculated the solvent effects by adding one/two explicit water molecules in the vicinity of the reactive center. The energy values are listed in Table 3, and the optimized geometries are given in the Supporting Information (Figures S9, S10, and S11).

Table 3. Calculated overall energy barriers of the water-assisted pathways.

	TS2Rh	TS2Pd	TS2Pt	TS3Rh	TS3Pd	TS3Pt
$\Delta E_{1\ water}$[a] [kcal mol^{-1}]	20.6	21.1	20.1	14.1	18.9	10.7
$\Delta E_{2\ waters}$[a] [kcal mol^{-1}]	20.1	20.5	20.0	13.7	18.4	10.4

[a] All electronic energies were calculated relative to reactants 1 TM + H_2O_2.

The inclusion of the first water solvent located above the reactive center (Supporting Information) reduces the overall energy barriers of **TS2s** or **TS3s** by about 5 kcal mol^{-1}. However, the addition of the second water solvent only reduced the barriers by about 1 kcal mol^{-1}. Thus, the remaining water solvents may have a similar effect in decreasing the barrier height of the rate-determining step.

2.7. Comparison with Experiments

Neumann and co-workers investigated the olefin epoxidation by using noble-metal-substituted sandwich-type POMs with H_2O_2.[39] They indicated that the cleavage of the HO–OH bond in initial ligation or interaction of H_2O_2 with substituted transition metals formed the TM–OH–(μ-OOH) intermediate, and

that it determines the reactivity and selectivity. In particular, Rh^{III}-, Pd^{II}-, and Pt^{II}-substituted POM catalysts possessed similar reactivities. The geometric character of the TM–OH–(μ-OOH) intermediate is of great importance, as it enables us to propose two possible pathways for the activation of H_2O_2. The values of the calculated energy barriers in the H_2O_2 activation step are not only close to each other, but are also higher than the energy barriers of the oxygen-transfer step, which is in good agreement with the experimental observations.[39] Next, the TM–OH–(μ-OOH) intermediate transfers an oxygen atom to the olefin to form an epoxide and the catalyst. We find that the interaction between the noble metal and the peroxo unit plays an important role in lowering the energy barrier and the yield of the epoxide, which is in agreement with experimental results.[39] Furthermore, Neumann and co-workers indicated that four active oxygen sites can be attacked by H_2O_2, and that the three-metal-bonded O_{3M} position will be more reactive, owing to its relatively higher electrophilicity. However, on the basis of our calculation results, owing to the higher stereoscopic hindrances of the O_{3M} position and the higher energy values of the TM–OH–(μ-O_{3M}OH) intermediates, the O_{2M} position is more favorable than the O_{3M} position. Therefore, future work should focus on decorating the central noble-metal atom and the coordination environment of the catalytic center.

3. Conclusions

The cyclohexene epoxidation mechanism has been investigated by using noble-metal-substituted sandwich-type POMs $\{[WZnTM_2(H_2O)_2](ZnW_9O_{34})_2\}^{n-}$ (TM=Rh^{III}, Pd^{II}, and Pt^{II}) with H_2O_2 at the B3LYP level. We achieved some important results, which are detailed as follows:

1) Two steps are proposed to describe the mechanism of olefin epoxidation: activation of H_2O_2 (step 1) and oxygen transfer (step 2). We found that aqua-coordinated POM has two novel pathways for the activation of H_2O_2 to form the TM–OH–(μ-OOH) intermediate. Step 1a, the dissociation of water molecule, and then the cleavage of HO–OH bond, or step 1b, cleavage of the HO–OH bond accompanied with H abstraction and OH addition. Step 1b is more facile, but it is also the rate-limiting pathway, and the similar energy barriers of the three catalysts are in good agreement with experimental results.
2) When we compare the three POMs, the Rh-containing POM becomes more competitive, because of the increased interactions between Rh^{III} and the peroxo unit.
3) Through the analysis of all active oxygen positions, we found that the O_{2M} position is more favorable than the O_{3M} position. O_{2M}–W is preferred for Rh- and Pd-containing POMs, whereas the O_{2M}–Zn position is slightly favored for the Pt-containing POM, suggesting that the future design of catalysts should focus on improving the coordination environment of reactive center.
4) When one and two water solvent molecules are present in the reactive system, the increased hydrogen bonding significantly reduces the energy barriers.

Computational Details

All calculations were carried out by using the Gaussian 09 A.02 software package and NBO program (version 3.1).[45,46] The geometries were fully optimized at the B3LYP level without any symmetry constraints.[47–49] For Rh, Pd, Pt, Zn, and W atoms, the LANL2DZ pseudopotential was added.[50] The 6–31 g (d,p) basis set was used for the reaction center, that is, H_2O_2 and C_6H_{10}, as well as C, H, O atoms that directly link with the central metals.[51–53] For the rest of the atoms, the 6–31g basis set was used.[51–53] Normal-mode frequency analysis was performed at the same level to characterize the nature of each stationary point. The local minima possess all real frequencies. The transition states were identified by the only one imaginary frequency and the normal modes that correspond to the expected reaction path. H_2O solvent was included in all corresponding calculations by using the polarized continuum model (PCM).[54] A very tight convergence (10^{-8} au) criterion was employed in all calculations. To evaluate the effect of explicit solvent, all reactants were fully optimized; whereas, in the transition states (O_{2M}–Zn position), the central reaction coordinates including TM–O, O–O, O–C, and O–H from the corresponding transition states were kept frozen.

Acknowledgements

The authors gratefully acknowledge financial support from the NSFC (21571031), the Foundation for University Key Teacher of Heilongjiang Province of China (1253G005), the Doctoral Scientific Research Foundation of Daqing Normal University (11ZR01), the Reserve Talents of Universities Overseas Research Program of Heilongjiang.

Keywords: catalysis · density functional calculations · epoxidation · mechanism · polyoxometalates

[1] G. De Faveri, G. Ilyashenko, M. Watkinson, *Chem. Soc. Rev.* **2011**, *40*, 1722 – 1760.
[2] H. Srour, P. Le Maux, S. Chevance, G. Simonneaux, *Coord. Chem. Rev.* **2013**, *257*, 3030 – 3050.
[3] O. A. Kholdeeva in *Liquid Phase Oxidation via Heterogeneous Catalysis: Organic Synthesis and Industrial Applications* (Eds.: M. G. Clerici, O. A. Kholdeeva), Wiley, New York, **2013**, chap. 4.
[4] O. A. Kholdeeva, *Catal. Sci. Technol.* **2014**, *4*, 1869 – 1889.
[5] S. S. Wang, G. Y. Yang, *Chem. Rev.* **2015**, *115*, 4893 – 4962.
[6] G. Strukul, *Catalytic Oxidations with Hydrogen Peroxide as Oxidant*, Kluwer, Dordrecht, **1992**.
[7] B. S. Lane, K. Burgess, *Chem. Rev.* **2003**, *103*, 2457 – 2474.
[8] R. Noyori, M. Aoki, K. Sato, *Chem. Commun.* **2003**, 1977 – 1986.
[9] N. Mizuno, K. Yamaguchi, K. Kamatab, *Coord. Chem. Rev.* **2005**, *249*, 1944 – 1956.
[10] K. Wendler, J. Thar, S. Zahn, B. Kirchner, *J. Phys. Chem. A* **2010**, *114*, 9529 – 9536.
[11] X. Luo, P. R. Fleming, T. R. Rizzo, *J. Chem. Phys.* **1992**, *96*, 5659 – 5667.
[12] X. López, J. J. Carbó, C. Bo, J. M. Poblet, *Chem. Soc. Rev.* **2012**, *41*, 7537 – 7571.
[13] X. López, P. Miró, J. J. Carbó, A. Rodríguez-Fortea, C. Bo, J. M. Poblet, *Theor. Chem. Acc.* **2011**, *128*, 393 – 404.
[14] J. M. Poblet, X. López, C. Bo, *Chem. Soc. Rev.* **2003**, *32*, 297 – 308.
[15] C. Venturello, R. D'Aloisio, *J. Org. Chem.* **1983**, *48*, 3831 – 3833.
[16] C. Venturello, R. D'Aloisio, J. C. J. Bart, M. Ricci, *J. Mol. Catal.* **1985**, *32*, 107 – 110.
[17] C. Venturello, M. Gambaro, *J. Org. Chem.* **1991**, *56*, 5924 – 5931.
[18] K. Kamata, K. Yonehara, Y. Sumida, K. Yamaguchi, S. Hikichi, N. Mizuno, *Science* **2003**, *300*, 964 – 966.

[19] A. Sartorel, M. Carraro, A. Bagno, G. Scorrano, M. Bonchio, *Angew. Chem. Int. Ed.* **2007**, *46*, 3255 – 3258; *Angew. Chem.* **2007**, *119*, 3319 – 3322.
[20] Y. Nakagawa, N. Mizuno, *Inorg. Chem.* **2007**, *46*, 1727 – 1736.
[21] X. Q. Huang, X. M. Zhang, D. Zhang, S. Yang, X. Feng, J. K. Li, Z. G. Lin, J. Cao, R. Pan, Y. N. Chi, B. Wang, C. Hu, *Chem. Eur. J.* **2014**, *20*, 2557 – 2564.
[22] G. Trautwein, B. El Bakkali, J. Alcaniz-Monge, B. Artetxe, S. Reinoso, J. M. Gutierrez-Zorrilla, *J. Catal.* **2015**, *331*, 110 – 117.
[23] J. Li, J. P. Guo, J. G. Jia, P. T. Ma, D. D. Zhang, J. P. Wang, J. Y. Niu, *Dalton Trans.* **2016**, *45*, 6726 – 6731.
[24] A. E. Kuznetsov, Y. V. Geletii, C. L. Hill, K. Morokuma, D. G. Musaev, *Inorg. Chem.* **2009**, *48*, 1871 – 1878.
[25] R. Prabhakar, K. Morokuma, C. L. Hill, D. G. Musaev, *Inorg. Chem.* **2006**, *45*, 5703 – 5709.
[26] N. S. Antonova, J. J. Carbo ', U. Kortz, O. A. Kholdeeva, J. M. Poblet, *J. Am. Chem. Soc.* **2010**, *132*, 7488 – 7497.
[27] P. Jiménez-Lozano, I. D. Ivanchikova, O. A. Kholdeeva, J. M. Poblet, J. J. Carbó, *Chem. Commun.* **2012**, *48*, 9266 – 9269.
[28] I. Y. Skobelev, O. V. Zalomaeva, O. A. Kholdeeva, J. M. Poblet, J. J. Carbó, *Chem. Eur. J.* **2015**, *21*, 14496 – 14506.
[29] P. Jiménez-Lozano, I. Y. Skobelev, O. A. Kholdeeva, J. M. Poblet, J. J. Carbó, *Inorg. Chem.* **2016**, *55*, 6080 – 6084.
[30] C. M. Tourné, G. F. Tourné, F. Zonnevijlle, *J. Chem. Soc. Dalton Trans.* **1991**, 143 – 155.
[31] A. R. Howells, A. Sankarraj, C. Shannon, *J. Am. Chem. Soc.* **2004**, *126*, 12258 – 12559.
[32] A. M. Morris, O. P. Anderson, R. G. Finke, *Inorg. Chem.*, **2009**, *48*, 4411 – 4420.
[33] P. T. Witte, S. R. Chowdhury, J. E. ten Elshof, D. Sloboda-Rozner, R. Neumann, P. L. Alsters, *Chem. Commun.* **2005**, 1206 – 1208.
[34] F. Hussain, B. S. Bassil, U. Kortz, O. A. Kholdeeva, M. N. Timofeeva, P. de Oliveira, B. Keita, L. Nadjo, *Chem. Eur. J.* **2007**, *13*, 4733 – 4742.
[35] R. Neumann, M. Gara, *J. Am. Chem. Soc.* **1994**, *116*, 5509 – 5510.
[36] R. Neumann, M. Gara, *J. Am. Chem. Soc.* **1995**, *117*, 5066 – 5074.
[37] R. Neumann, A. M. Khenkin, *Inorg. Chem.* **1995**, *34*, 5753 – 5760.
[38] R. Neumann, A. M. Khenkin, *J. Mol. Catal. A: Chem.* **1996**, *114*, 169 – 180.
[39] R. Neumann, A. M. Khenkin, D. Juwiler, H. Miller, M. Gara, *J. Mol. Catal. A: Chem.* **1997**, *117*, 169 – 183.
[40] S. R. Amanchi, A. M. Khenkin, Y. Diskin-Posner, R. Neumann, *ACS Catal.* **2015**, *5*, 3336 – 3341.
[41] R. R. Sever, T. W. Root, *J. Phys. Chem. B* **2003**, *107*, 4080 – 4089.
[42] R. R. Sever, T. W. Root, *J. Phys. Chem. B* **2003**, *107*, 4090 – 4099.
[43] R. R. Sever, T. W. Root, *J. Phys. Chem. B* **2003**, *107*, 10521 – 10530.
[44] D. V. Deubel, G. Frenking, P. Gisdakis, W. A. Herrmann, N. Rösch, J. Sundemeyer, *Acc. Chem. Res.* **2004**, *37*, 645 – 652.
[45] E. D. Glendening, A. E. Reed, J. E. Carpenter, F. Weinhold, NBO Version 3.1, Gaussian 09, Gaussian, Inc., Wallingford, CT, **2009**.
[46] M. J. Frisch, G. W. Trucks, H. B. Schlegel, G. E. Scuseria, M. A. Robb, J. R. Cheeseman, G. Scalmani, V. Barone, B. Mennucci, G. A. Petersson, H. Nakatsuji, M. Caricato, X. Li, H. P. Hratchian, A. F. Izmaylov, J. Bloino, G. Zheng, J. L. Sonnenberg, M. Hada, M. Ehara, K. Toyota, R. Fukuda, J. Hasegawa, M. Ishida, T. Nakajima, Y. Honda, O. Kitao, H. Nakai, T. Vreven, J. A. Montgomery, Jr., J. E. Peralta, F. Ogliaro, M. Bearpark, J. J. Heyd, E. Brothers, K. N. Kudin, V. N. Staroverov, R. Kobayashi, J. Normand, K. Raghavachari, A. Rendell, J. C. Burant, S. S. Iyengar, J. Tomasi, M. Cossi, N. Rega, J. M. Millam, M. Klene, J. E. Knox, J. B. Cross, V. Bakken, C. Adamo, J. Jaramillo, R. Gomperts, R. E. Stratmann, O. Yazyev, A. J. Austin, R. Cammi, C. Pomelli, J. W. Ochterski, R. L. Martin, K. Morokuma, V. G. Zakrzewski, G. A. Voth, P. Salvador, J. J. Dannenberg, S. Dapprich, A. D. Daniels, Ö. Farkas, J. B. Foresman, J. V. Ortiz, J. Cioslowski, D. J. Fox, Gaussian 09, Revision A.1, Gaussian, Inc., Wallingford CT, **2009**.
[47] C. Lee, C. Yang, R. G. Parr, *Phys. Rev. B* **1988**, *37*, 785 – 789.
[48] A. D. Becke, *J. Chem. Phys.* **1993**, *98*, 5648 – 5652.
[49] P. J. Stephens, F. J. Devlin, C. F. Chabalowski, M. J. Frisch, *J. Phys. Chem.* **1994**, *98*, 11623 – 11627.
[50] P. J. Hay, W. R. Wadt, *J. Chem. Phys.* **1985**, *82*, 270 – 283.
[51] M. M. Francl, W. J. Pietro, W. J. Hehre, J. S. Binkley, M. S. Gordon, D. J. Defrees, J. A. Pople, *J. Chem. Phys.* **1982**, *77*, 3654 – 3665.
[52] W. J. Hehre, R. Ditchfield, J. A. Pople, *J. Chem. Phys.* **1972**, *56*, 2257 – 2261.
[53] P. C. Hariharan, J. A. Pople, *Theor. Chim. Acta.* **1973**, *28*, 213 – 222.
[54] E. Cancès, B. Mennucci, J. Tomasi, *J. Chem. Phys.* **1997**, *107*, 3032 – 3041.

Received: June 17, 2016
Published online on September 30, 2016

